Magnetic field estimation in measurement dead domain for dry calibration of electromagnetic flowmeter

2012 Meas. Sci. Technol. 23 085303

(http://iopscience.iop.org/0957-0233/23/8/085303)

Meas. Sci. Technol. **23** (2012) 085303 (9pp) doi:10.1088/0957-0233/23/8/085303

Magnetic field estimation in measurement dead domain for dry calibration of electromagnetic flowmeter

L Hu[1], H M Shen[1], K M Lee[2,3] and X Fu[1]

[1] State Key Laboratory of Fluid Power Transmission and Control, Zhejiang University, Hangzhou, People's Republic of China
[2] Woodruff School of Mechanical Engineering, Georgia Institute of Technology, Atlanta, GA 30332-0405, USA
[3] School of Mechanical Engineering, Huazhong University of Science and Technology, Wuhan, People's Republic of China

E-mail: xfu@zju.edu.cn

Received 12 November 2011, in final form 10 May 2012
Published 14 June 2012
Online at stacks.iop.org/MST/23/085303

Abstract
Advances in computing technology enable dry calibration of large-diameter electromagnetic (EM) flowmeters at low cost, which has been recognized as an effective alternative to traditional flow rigs. Dry calibration requiring no actual liquid in the measuring pipe utilizes the magnetic field distribution reconstructed from measured boundary conditions to determine the sensitivity of the EM flowmeter. However, because sensors have finite sizes, and the fact that inner linings of the measuring pipe deform due to mechanical stresses, a measurement dead domain (MDD) exists between the measured boundary surface and the pipe wall. As the MDD is often close to the magnetic exciting unit, neglecting it results in significant errors in dry calibration. This paper offers a practical method combining iterative optimization and reconstruction to estimate the magnetic field in the MDD from the field data on the measured boundary surface. The method has been validated on an off-the-shelf industrial EM flowmeter by comparing the estimated field in the MDD with experimental measurements. It has been demonstrated that accurately accounting for the immeasurable field in the MDD eliminates more than two-thirds of the dry calibration errors. The estimation method illustrated here can also be extended to measure other physical fields which obey similar governing equations.

Keywords: electromagnetic flowmeter, dry calibration, magnetic field, reconstruction, optimization, measurement dead domain, estimation

(Some figures may appear in colour only in the online journal)

1. Introduction

The operational principle of an electromagnetic (EM) flowmeter is based on Faraday's law of induction to measure the flow rate of conductive liquid flowing through the magnetic field in the pipe [1]. Owing to their high precision with no pressure loss, lack of pollution and high reliability, EM flowmeters have been widely used in water systems and chemical plants in the last few decades [2]. To ensure product precision and reliability, commercial EM flowmeters are calibrated to meet standards (such as ISO 9104:1991 [3]) before leaving the factory or after a period of use. Due to the rapid growth in water demand (and thus increase in pipe diameters and flowmeter production), there is a need to develop new calibration methods as traditional flow rigs are time consuming, energy demanding and not *in situ* [4–6].

With widely available computing technologies at low cost, dry calibration has been recognized as an energy-saving alternative (especially for large EM flowmeters [5]) to traditional flow rigs, and a means to predict the flowmeter

performance for special flow structures. An accurate magnetic field distribution in the measuring pipe, which can be reconstructed by solving Laplace's equation of a scalar magnetic potential with measured boundary conditions (BCs), plays a significant role in dry calibration of an EM flowmeter. This method (combining the measurement and calculation) does not require information on the inner structure of the flowmeter and has high precision [5, 7–9]. Due to these advantages, dry calibration has been widely accepted by flowmeter manufactures and users in industries.

Flowmeters require periodic maintenance and recalibration as their inner surfaces (which, in many practical applications, are often covered with PTFE or rubber protective materials) may deform due to mechanical stress, fluid pressure and temperature of the fluid [2]. As a result, a small region (referred to here as the measurement dead domain or simply MDD) near the pipe wall is not measurable. There is a need to extend previously published dry calibration methods [5, 8], which have been developed for calibrating flowmeters before leaving factories, to account for the effects of the MDD (due to geometrical pipe-wall deformation) on dry calibration.

Estimation utilizing magnetic fields as a medium has been a common problem in many areas of study. In medical research, cerebral cortex activities are estimated from measured magneto-encephalogram signals corresponding to brain activities [10, 11]. Estimation is also needed in capsule endoscopy location [12] and digestive motility detection [13] in medical clinics. For rehabilitation, inertial and magnetic sensing data [14, 15] are used to estimate human motion trajectory. In industry, there are also multitudinous similar estimation problems based on detecting information, for example, position estimation of the EM servo system [16] and crack detection [17]. Parameter estimation is also often found in control system implementation of industrial machines [18–19]. An approach in solving parameter estimation problems is by means of an optimization algorithm (such as least-squares methods [20]) utilizing information related to the estimated source as an optimization object [10–13, 19]. In addition, modeling with unique solutions [16] and new approaches such as neural networks [18] and extended Kalman filter [14, 15] have also been proposed to solve the estimation problems.

This paper extends our previous studies [5, 8] to improve dry calibration of flowmeters that experience a long history of service. Specifically, it introduces an estimation method to cost effectively account for the immeasurable field in the MDD. The method combines iterative optimization and reconstruction, and takes advantages of the partially reconstructed field from the measured boundary to enhance the specification of the initial distribution. Different from the above studies where lumped parameter approaches were primarily used in optimization and interest was often in estimating localized information (such as source location and orientation), the problem studied here concerns accurate estimation of the magnetic field distribution in a domain, which involves a significant number of estimated parameters and the non-uniqueness of the inverse solution.

The remainder of this paper offers the following.

(1) A distributed-parameter method for estimating the magnetic field in the MDD is formulated as a large-scale-constrained optimization problem, which uses the magnetic field reconstructed from data measured on a virtual surface (away from the actual wall, i.e. the measured boundary) as a basis for estimating the commonly neglected field.
(2) The estimation method has been experimentally validated on an off-the-shelf industrial EM flowmeter, where the MDD geometry and flux density on the pipe wall are measured using a laser probe and a Hall probe, respectively. With the validated field, the effects of field approximations in the MDD on dry calibration are investigated. As will be shown, nearly two-thirds of the dry calibration error is eliminated by accurately taking into account the magnetic field in the MDD.

While discussed in the context of magnetic fields, the proposed method can be readily extended to other physical fields (such as electric, temperature). The method of utilizing the reconstructed partial field to provide additional object information and specify a proper initial can also be used to improve the estimation accuracy of other applications based on lumped-parameter approaches, for example, in the determination of the cerebral cortex activity as well as estimating the position of a magnetic capsule endoscope by reconstructing its induced field outside the human body.

2. Estimation method

In physics, any potential field obeying Laplace's equation is source free and can be uniquely determined when the BCs are well defined. This physical law provides a means to computationally reconstruct the field distribution in space with measured BCs [7].

Neglecting the current due to the motion of the conductive fluid [5, 7], the magnetic flux density **B** in the measuring pipe of EM flowmeter can be solved from Laplace's equation (1*a*) in terms of its scalar potential Ψ defined in (1*b*):

$$\nabla^2 \Psi = 0; \tag{1a}$$

$$\mathbf{B} = -\mu \nabla \Psi, \tag{1b}$$

where μ is the magnetic permeability of the fluid in the pipe. The required BCs may be a Dirichlet boundary condition (DBC) and/or a Neumann boundary condition (NBC) as specified in (2*a*), (2*b*), respectively:

$$\Psi|_{\Gamma_1} = \Psi_0; \tag{2a}$$

$$\left.\frac{\partial \Psi}{\partial n}\right|_{\Gamma_2} = -\frac{B_n}{\mu}. \tag{2b}$$

In the above equations, the subscripts (Γ_1 and Γ_2) denote different regions of the boundary surface, and B_n specifies the normal component of the magnetic flux density [5]. With a few exceptions (such as the magnetic ground surface or remote far field where Ψ can be reasonably approximated and arbitrarily set to zero), the potential Ψ is not measurable in practice [7]. The B_n distribution can be measured (by means

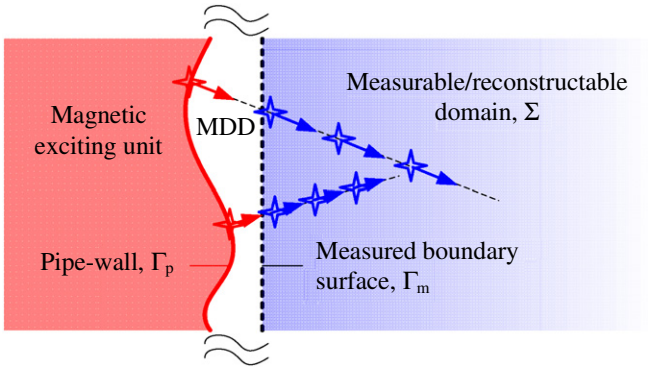

Figure 1. Illustration of the regions for the B_n distribution measurement.

of magnetic sensors such as a Hall sensor) providing the NBC to help specify the complete set of BCs required for solving (1*a*).

Figure 1 illustrates the field estimation problem, where the entire magnetic field (inside the circular pipe wall Γ_p) must be accurately modeled for dry calibration. Measurements are made on the surface Γ_m and the space between Γ_p and Γ_m is referred to here as the measurement dead domain (MDD). A finite number of discrete BC values c_i at the discrete locations (x_i, y_i, z_i) are expressed as a matrix in (3), where k is the number of points:

$$[\mathbf{C}] = \begin{bmatrix} x_1 & y_1 & z_1 & c_1 \\ x_2 & y_2 & z_2 & c_2 \\ x_3 & y_3 & z_3 & c_3 \\ & \cdots\ \cdots & & \\ x_i & y_i & z_i & c_i \\ & \cdots\ \cdots & & \\ x_k & y_k & z_k & c_k \end{bmatrix}, \quad 1 \leqslant i \leqslant k. \tag{3}$$

It is worth mentioning that the method presented here does not require any knowledge of the excitation unit or any mathematical closed-form expression to model Γ_p. However, very close to the excitation unit, a much higher magnetic flux density stored in the MDD than in domains near the pipe center is expected. For clarity in illustration, the magnetic flux density partially reconstructed from the measured BCs is denoted as $\hat{\mathbf{B}}(x, y, z, [\mathbf{C}]_m)$, while the estimated but complete magnetic flux density required for dry calibration is denoted as $\tilde{\mathbf{B}}(x, y, z, [\mathbf{C}]_p)$, where the subscripts '$m$' and '$p$' refer to data measured on a free surface Γ_m and data estimated at the actual pipe wall Γ_p, respectively. The former $\hat{\mathbf{B}}$ can be reconstructed from $[\mathbf{C}]_m$ using methods discussed in [7] and is assumed available for estimating $[\mathbf{C}]_p$ on the pipe wall in this study.

The estimation of $[\mathbf{C}]_p$ is formulated as an optimization problem that minimizes the difference between $\tilde{\mathbf{B}}(x, y, z, [\mathbf{C}]_p)$ and $\hat{\mathbf{B}}(x, y, z, [\mathbf{C}]_m)$ as an objective function (4) subject to constraint (5) in the measurable reconstructed domain $\sum$:

$$\min_{\xi} \int_{\Sigma} \|\tilde{\mathbf{B}}(x, y, z, [\mathbf{C}]_p) - \hat{\mathbf{B}}(x, y, z, [\mathbf{C}]_m)\|^2 \, \mathrm{d}\Sigma \tag{4}$$

$$\int_{\Gamma_p} B_n(x, y, z, [\mathbf{C}]_p) \, \mathrm{d}\Gamma_p = 0. \tag{5}$$

Since B_n passing through Γ_p (that encloses the entire source-free domain) is zero, constraint (5) must be strictly obeyed during optimization as it is the solvability condition of (1*a*).

The sequential quadratic programming (SQP) method, which has been proven highly effective for solving large-scale constrained optimization problems with smooth nonlinear objective functions [21], is employed here to solve (4) using a sequence of quadratic programming (QP) sub-problems. The algorithm consists of major and minor iterations. The major iterations satisfying the linear constraints converge to a point that satisfies the nonlinear constraints and first-order conditions for optimality, each of which reconstructs the complete field with BCs specified at the pipe wall. A QP sub-problem is then used to generate a search direction toward the next iteration [21]. The SQP has been implemented using the toolbox SNOPT as well as a computing program specifically written for the reconstruction. The solution to (4) involves the following two considerations, which are separately discussed in subsections 2.1 and 2.2.

2.1. Non-uniqueness of the model solution

For a given $[\mathbf{C}]_m$, constraint (5) implies that the estimated $[\mathbf{C}]_p$ on the pipe wall must satisfy (6) to ensure that Laplace's equation for the MDD is satisfied:

$$\int_{\Gamma_p} [\mathbf{C}]_p \, \mathrm{d}\Gamma_p + \int_{\Gamma_m} [\mathbf{C}]_m \, \mathrm{d}\Gamma_m = 0. \tag{6}$$

In practice, there are infinite possible BC distributions $[\mathbf{C}]_p + \Delta[\mathbf{C}]_p$ on the pipe wall obeying (6) as long as $\int_{\Gamma_p} \Delta[\mathbf{C}]_p \mathrm{d}\Gamma_p = 0$ on it. As different BCs yield a particular field distribution in the MDD, the solutions to (4) are thus non-unique.

2.2. Initialization using extrapolation with orthogonal properties

Due to possible non-unique solutions mentioned above as well as the need to determine a large number of variables in (3), an appropriate initial guess is essential so that a correct optimal solution can be found with little iterations. This is particularly important since SQP yields only locally optimal solutions. To overcome these problems, the initial $[\mathbf{C}]_p$ guess is obtained by extrapolating the reconstructed $\hat{\mathbf{B}}(x, y, z, [\mathbf{C}]_m)$ as illustrated in figure 1 where several equally spaced data points are extrapolated to estimate the points on the pipe wall. The required number of points for extrapolation depends on the methods such as linear, cubic spline or least squares. This study specifies the data positions utilizing the orthogonal property of the curl-free magnetic field, i.e. a function f obeying Laplace's equation can be separated (separation of variables [22]) into three independent functions $A(\alpha)$, $B(\beta)$ and $G(\gamma)$ in the orthogonal (Cartesian, cylindrical or spherical) coordinates (α, β, γ):

$$f(\alpha, \beta, \gamma) = A(\alpha) \, B(\beta) \, G(\gamma). \tag{7}$$

In practice, **B** or the gradient of the scalar potential in (1*b*) is measured. As an illustration, consider a 2D field in

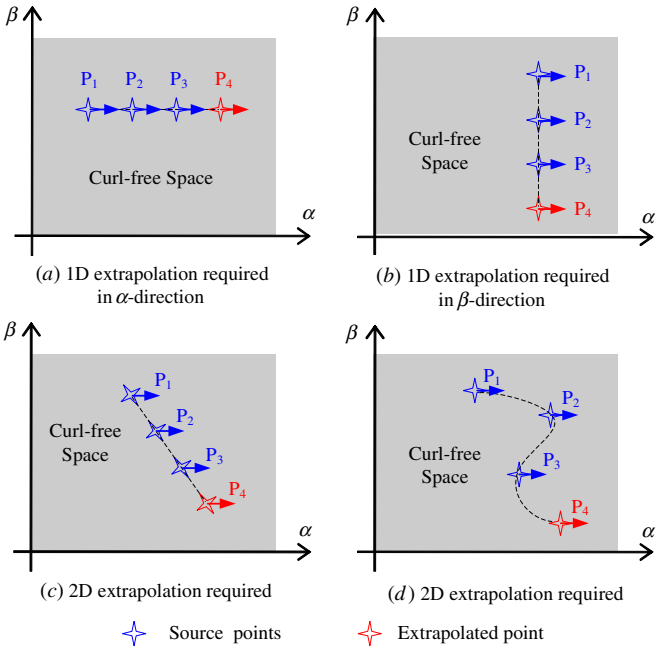

Figure 2. Illustration of the vector extrapolation in 2D space.

figure 2, where the field vector at P_4 is extrapolated from the data P_1, P_2 and P_3 along the α-axis. In 2D, the derivative of f with respect to the α-axis (denoted as F_α) can be formulated as

$$F_\alpha(\alpha,\ \beta) = A'(\alpha)\, B(\beta), \tag{8}$$

where $A'(\alpha)$ is the derivative of A in the α-direction. Unlike 1D extrapolations in the α or β directions as shown in figures 2(*a*) and (*b*), the straight line in figure 2(*c*) requires 2D extrapolation as it is not parallel to any axis. In figure 2(*d*), where the point locations are not on a well-defined straight or circular line, such 2D computationally complex extrapolation generally yields poor precision and is avoided. Based on the above considerations and the fact that the B_n data are required on the pipe wall, the source points are chosen along the normal for estimating B_n on the pipe wall as illustrated in figure 1.

3. Results and discussion

For validating the estimated magnetic field in the MDD and for improving the precision of dry calibration, the method has been implemented on an off-the-shelf industrial EM flowmeter, which has deformed inner surfaces after a long history of services in measuring the flow rate of hot liquid.

3.1. Experimentally measured surface morphology

Figure 3(*a*) shows the experimental setup for dry calibrating the flowmeter with a nominal inner radius of 100 mm, where a Hall probe driven by a scanning servo mechanism was used to measure the B_n distribution on the pipe wall. The scanning servo mechanism moved the Hall sensor from one point to the next when taking a measurement, which requires 0.5 s to travel a maximum distance of 15 mm (or an average speed of 30 mm s^{-1}) and an additional 0.1 s (or 5 time constants of

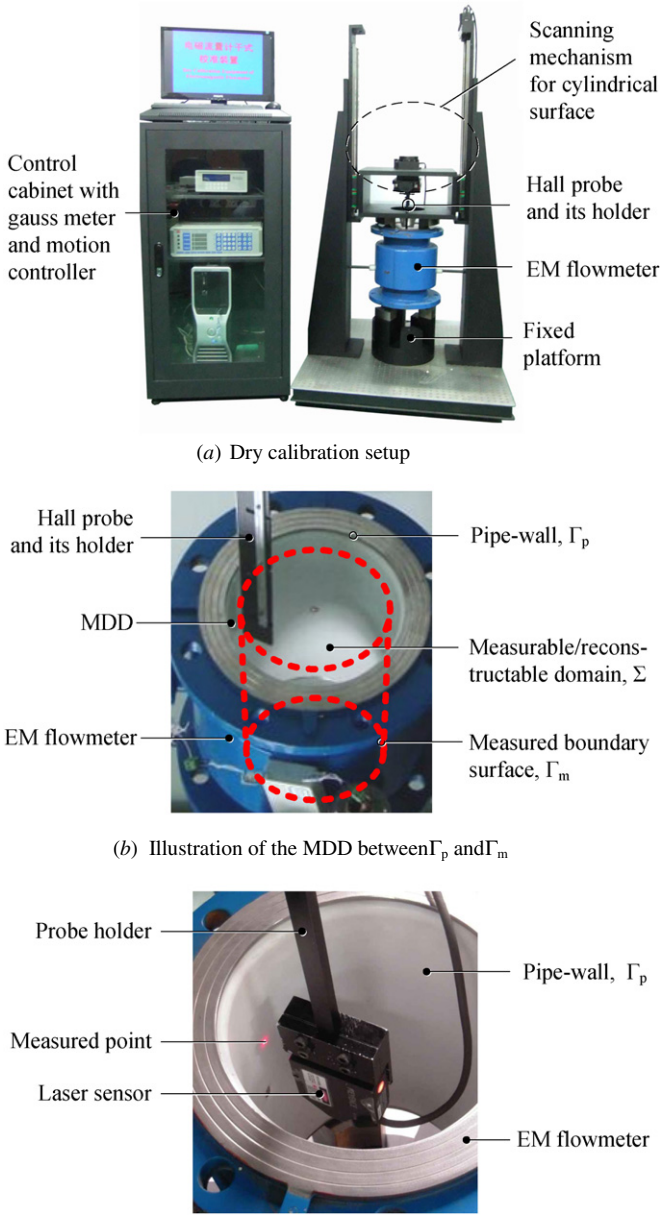

Figure 3. Space geometrical measurement of MDD on the dry calibration setup.

Table 1. Geometry parameters of the EM flowmeter and the MDD (along the length of the flowmeter: 0–300 mm).

Parameters	Values
Nominal inner radius of the flowmeter	100 mm
Scanning radius of the Hall probe	92 mm
Actual inner radius of the flowmeter	95.5–104.2 mm
Depth of the MDD in the radius direction	3.5–12.2 mm

the gauss meter) for the sensor to read a static measurement. The geometrical characteristics are summarized in table 1 and figure 4.

To avoid collision during scanning with the magnetic sensor, the Hall probe is scanned circumferentially with a radius of 92 mm as illustrated in figure 3(*b*). Pulsed dc currents

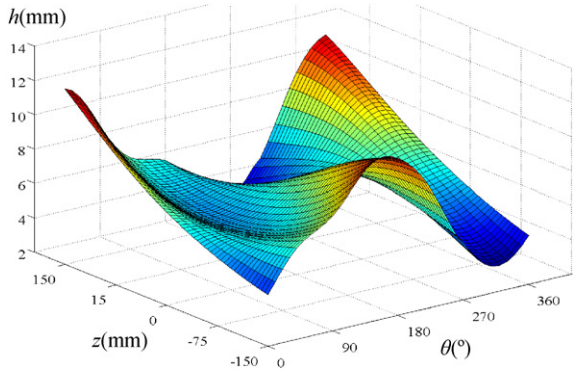

Figure 4. Measured MDD geometry.

exciting alternating magnetic field are used in actual EMFs to avoid polarization effects on the electrodes. Here, the pulsed-dc exciting current is transformed to a constant-dc current, and accordingly builds a static magnetic field in the measuring pipe for easy measurement. The static field has the same strength and distribution with the alternating field, and will not cause polarization on electrodes because no water is filled in the pipe during dry calibration [7]. The actual morphology of the pipe wall is determined by a servo-driven laser displacement sensor as shown in figure 3(*c*). The measurements reveal that the inner radius varies somewhat from 95.5 to 104.2 mm and that the MDD has a depth variation of 3.5–12.2 mm.

3.2. Partial magnetic field reconstructed from measured data

Figure 5(*a*) shows the measured BCs at the radius 92 mm, for which the 3D magnetic flux density $\hat{\mathbf{B}}$ is reconstructed by solving (1*a*) with measured $[\mathbf{C}]_m$. A typical reconstructed $\hat{\mathbf{B}}$ on the *x*–*y* plane is plotted in figure 5(*b*) showing that the field magnitude near the pipe wall is larger than that in the center.

3.3. Estimation of initial BCs at the pipe wall

Once the discrete points on the pipe wall are specified by the laser measurement (figure 5), the magnetic flux density at each of these points along its normal can be extrapolated from the reconstruction. As illustrated in figure 6, P_1 to P_9 are the laser-scanned discrete points on the pipe wall, where P_5 surrounded by eight neighbor triangles (T_1 to T_8) is their center and $\boldsymbol{n}_1$ to $\boldsymbol{n}_8$ are the normals of the eight triangular planes. The normals can be calculated from (9), where the subscripts (*a*, *b* and *c*) denote the vertex point P of a triangle:

$$\mathbf{n}_i = \overline{\mathrm{P}_a\mathrm{P}_b} \times \overline{\mathrm{P}_a\mathrm{P}_c} = \begin{vmatrix} \vec{x} & \vec{y} & \vec{z} \\ x_b - x_a & y_b - y_a & z_b - z_a \\ x_c - x_a & y_c - y_a & z_c - z_a \end{vmatrix}. \quad (9)$$

The normal $\bar{\mathbf{n}}$ at P_5 is the average of $\boldsymbol{n}_1$–$\boldsymbol{n}_8$:

$$\bar{\mathbf{n}} = \frac{1}{8}\sum_{i=1}^{8} \mathbf{n}_i. \quad (10)$$

In figure 6, the projections of P_1–P_9 (P'_1–P'_9) are equally spaced in the θ and z directions. For the points on the boundary, only four triangles are calculated. For example, the normal on the boundary point P_2 is the average of the normal of the

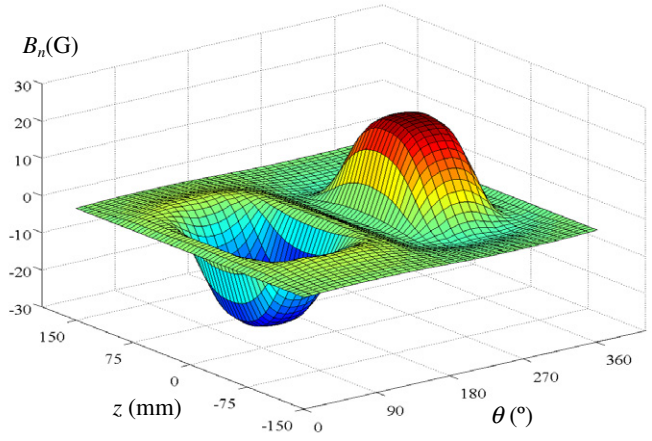

(*a*) Measured BC on the cylindrical surface ρ=92mm

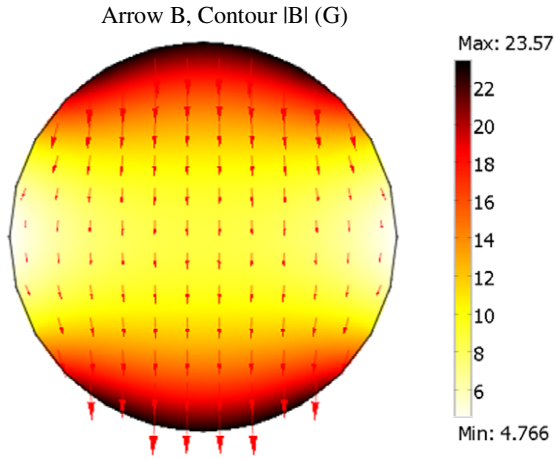

(*b*) Slice contour and vector arrows of reconstructed **B** at *z*=0mm

Figure 5. Illustration of the partial field reconstruction.

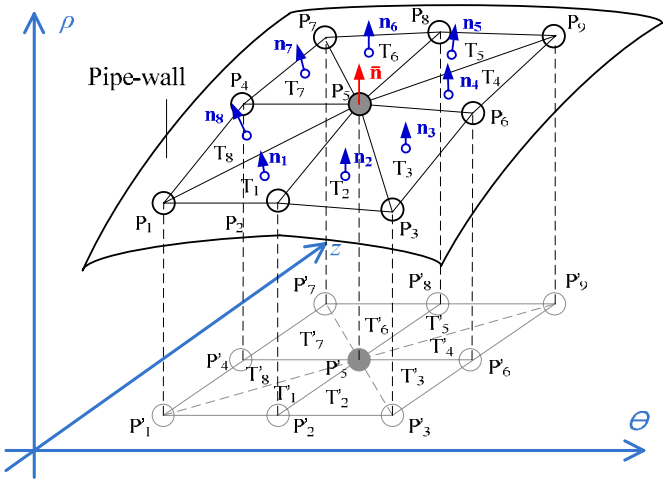

Figure 6. Computation of the normal direction on discrete points.

four triangles with vertexes (P_1, P_2, P_4), (P_2, P_5, P_4), (P_2, P_6, P_5) and (P_2, P_3, P_6). Using (9) and (10), the normal for each measured point can be calculated. Figure 7 shows the three source surfaces (first, second and third) as well as the normals of several points at $\theta = 290°$, which exhibit somewhat

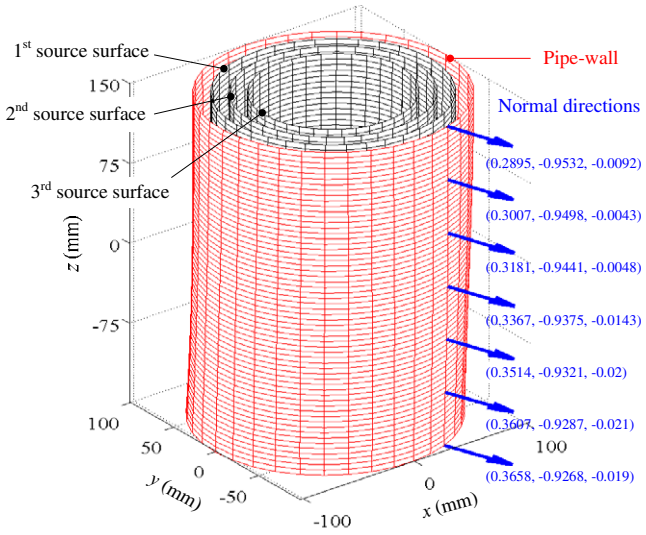

Figure 7. Source surfaces for extrapolation.

Table 2. Convergence history.

Step, n	Self-residual	Relative error
0	—	15
1	0.115	3.95
2	0.030	1.01
3	0.007	0.32
4	0.002	0.12
5	0.0006	0

different directions because of the pipe surface irregularity. Figures 8(*a*)–(*c*) and (*d*) graph the reconstructed field on the three source surfaces and the extrapolated initial BC guess on the pipe wall, respectively.

3.4. Validation of optimized results

As shown in table 2 where

$$\text{residual} = (B_{\text{Max}_n} - B_{\text{Max}_{n-1}})/B_{\text{Max}n}$$

$$\text{relative difference} = 100\% \times (B_{\text{Max}_n} - B_{\text{Max}_5})/B_{\text{Max}_5}$$

and B_Max denotes the magnitude of the BC distribution, the optimization takes five iterations to converge to a residual of less than 10^{-3}, reducing the maximum error to about 15% (figure 9).

The estimation has been validated experimentally using Hall sensors attached on the pipe wall measuring the local normal flux density as shown in figure 10(*a*). As compared in figure 10(*b*), the estimated and measured data (at $z = 0$ and 50 mm) show excellent agreement with each other. With the estimated BCs on the pipe wall, the complete field distribution including those in the MDD has been reconstructed. To quantify the relative weight of the commonly neglected or roughly assumed magnetic field near the pipe wall, the field energy integral $\int_V B^2/\mu \, dV$ in the MDD is compared with that in the domain Σ (or the interior region of the pipe but neglecting the MDD as shown in figure 1) in table 3. The findings show that although the volume of the MDD is only

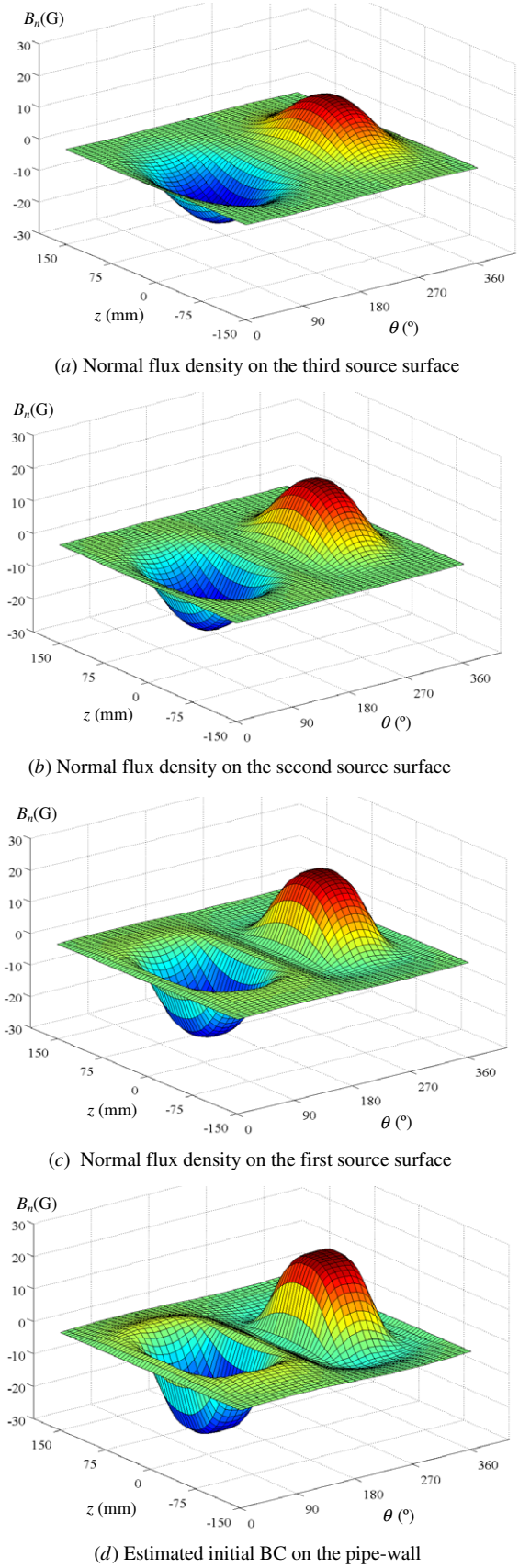

(*a*) Normal flux density on the third source surface

(*b*) Normal flux density on the second source surface

(*c*) Normal flux density on the first source surface

(*d*) Estimated initial BC on the pipe-wall

Figure 8. Determination of the initial BC on the pipe wall through extrapolation.

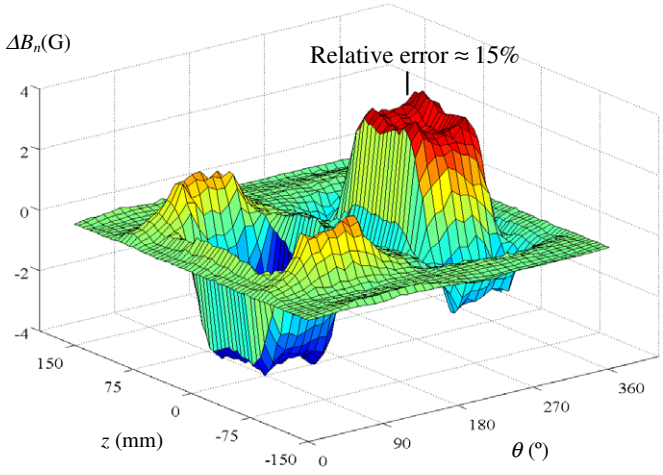

Figure 9. Eliminated error through the iterative optimization computation.

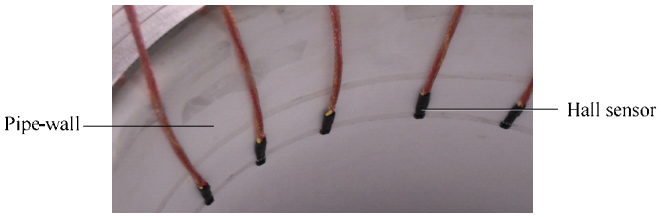

(*a*) Experimental measurement of BC on pipe-wall with Hall sensors

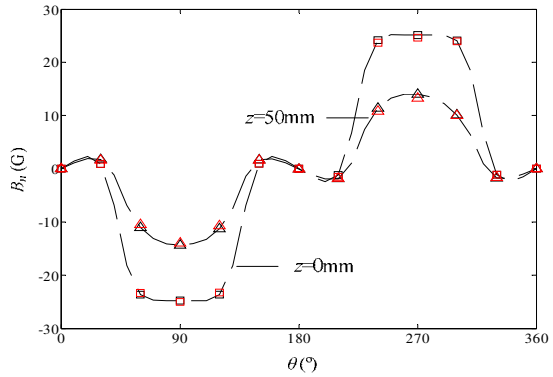

(*b*) Comparison between the estimated (black) and measured (red) data

Figure 10. Experimental validation of the estimated BC on the pipe wall.

Table 3. Comparison of magnetic energy.

Compared items	Ratio value (MDD: Σ)
Volume	1.0 : 6.2
Magnetic energy	1.0 : 2.8
Average energy density	2.2 : 1.0

one-sixth of the domain Σ the average energy density in the MDD is more than double that in Σ.

3.5. Illustrative application to dry calibration

Dry calibration of an EM flowmeter determines its sensitivity S defined in (11*a*), which is the induced voltage ΔU between the electrodes divided by the average fluid flow velocity **v**:

$$S = \frac{\Delta U}{\bar{v}}, \tag{11a}$$

where

$$\Delta U = \int_{\Omega} \mathbf{v}(\mathbf{B} \times \mathbf{W})\, \mathrm{d}\Omega. \tag{11b}$$

In (11*b*), Ω is the measuring volume, and the weight function **W** characterizes the contribution of the induced voltage at different positions in the volume. The method to solve for the field distributions of **v**, **B** and **W** in Ω from a coupled set of multi-physical equations with measured BCs can be found in [7].

The effects of the MDD field on the dry calibration are examined using integral (11) by comparing the results of the proposed estimation method with an approximation assuming that the field in the MDD is in the radial direction everywhere with values equal to the measured data on the MBS. As shown in equation (11*b*), any change in computation geometry, weight function and magnetic field could affect the results of dry calibration. Thus, the same actual measured wall geometry was used in both cases (estimation and approximation). However, the actual field in MDD is a complex 3D vector field; in fact, the magnetic flux in the MDD near the magnetic exciting unit is denser (hence higher magnetic flux density) than that on the MBS. Thus, it is expected that the assumption that equates the MDD field to the measured MBS field would tend to compromise the precision of the dry calibration.

Dry calibration accurately accounting for the magnetic field in the MDD was carried out for the case where water (at a velocity of 5 m s^{-1}) flows through the flowmeter mounted between two straight 3 m pipes upstream and downstream to ensure that the flow is fully developed. In both cases (proposed estimation and approximation), the new accurately measured pipe wall geometry is used as shown in figure 3 to eliminate possible effects from the differences in the computation geometry and weight function. As given in table 4, the sensitivity value S (defined in equation 11) was determined by the flow-rig experiment and the two dry calibrations (using the estimation method or not) in this flow condition. The relative error between the flow-rig-calibrated sensitivity S_D and dry-calibrated sensitivity S_F was calculated to validate the improvement of the dry calibration brought by the proposed estimation method. In the flow-rig experiment, we used the weight scale method whose uncertainty is 0.05% to determine the average velocity $\bar{v}$ actually passing through the tested flowmeter. To ensure enough precision, the voltage ΔU induced between the electrodes by the flow was amplified 1000 times through a standard EMF signal processing unit and then measured by a digital voltage-meter whose maximum measuring error was 0.1 μV, i.e. the measuring resolution of the induced voltage was 0.0001 μV. As shown in the table, the relative error between the dry calibration result and flow-rig calibration (using real fluid) was reduced from 1.05% to 0.32%, i.e. 69.5% of the calibration error was eliminated by improving the estimation of the MDD field. This is a significant improvement for the dry calibration technology, especially when calibrating a flowmeter with a very large diameter.

Table 4. Comparison between flow-rig and dry calibrations at flow velocity 5 m s^{-1}.

Is the estimation method used?	Flow-rig calibrated sensitivity, S_F (mV/(m s^{-1}))	Dry calibrated sensitivity, S_D (mV/(m s^{-1}))	Relative error $\left\|\frac{S_D-S_F}{S_F}\right\| \times 100\,\%$
No	0.110 904 (with uncertainty of 0.05%)	0.109 739	1.05
Yes		0.110 549	0.32

4. Conclusion

A method for estimating the commonly neglected or roughly assumed magnetic field distribution in the MDD has been presented for improving dry calibration of an EM flowmeter. Formulated mathematically as a large-scale constrained optimization problem, the method combining iterative optimization and magnetic field reconstruction improves the magnetic field model required for calculating the sensitivity of an EM flowmeter. It has been shown that the partially reconstructed field provided additional object information and gave a good initial distribution through extrapolation for estimating the BCs on the pipe wall, which enables the SQP algorithm to converge in a few iterations.

The method has been applied on an off-the-shelf industrial flowmeter (with a diameter of 100 mm), and validated experimentally by measuring the MDD geometry and the magnetic field on the pipe wall. Measurement results show that the depth of the MDD varies from 3.5 to 12.2 mm. Although the MDD has a relatively small volume, its average energy density is more than twice that in the remaining pipe interior. The estimated BC agrees well with the experimentally measured results using Hall sensors adhered to the pipe wall.

Finally, the dry calibration with data that accurately account for the field in the MDD removes 69.5% of its error. As compared with standard flow rigs, the relative error in the dry calibration reduces from 1.05% to 0.32%, a significant potential to advance the dry calibration technology. It is also expected that the estimation method illustrated here can be extended to measure other physical fields which obey similar governing equations. The idea of taking advantage of partial field to provide additional object information and specify a proper initial through field reconstruction can also be used in other parameter estimation problems in medical and industry.

Acknowledgments

The authors are grateful to the financial support of the National Basic Research Program (973) of China (no 2011CB013300), the National Natural Science Foundation of China (no 51105329) and Postdoctoral Science Foundation of China (no 20100481416).

References

[1] Shercliff J A 1962 *The Theory of Electromagnetic* (London: Cambridge University Press)
[2] Baker R C 2000 *Flow Measurement Handbook* (London: Cambridge University Press)
[3] International Organization for Standardization 1991 Measurement of fluid flow in closed conduits—methods of evaluating the performance of electromagnetic flow-meters for liquids ISO 9104:1991
[4] Hemp J 2001 A technique for low cost calibration of large electromagnetic flowmeters *Flow Meas. Instrum.* **12** 123–34
[5] Fu X, Hu L, Lee K M, Zou J, Ruan X D and Yang H Y 2010 Dry calibration of electromagnetic flowmeters based on numerical models combining multiple physical phenomena (multiphysics) *J. Appl. Phys.* **108** 083908
[6] Baker R C 2011 On the concept of virtual current as a means to enhance verification of electromagnetic flowmeters *Meas. Sci. Technol.* **22** 105403
[7] Hu L, Lee K M and Fu X 2010 A method based on measured boundary conditions for reconstructing the magnetic field distribution of an electromagnetic mechatronic system *IEEE/ASME Trans. Mechatronics* **15** 595–602
[8] Hu L, Lee K M, Zou J, Fu X and Yang H Y 2010 Adaptive measurement for automated field reconstruction and calibration of magnetic systems *IEEE Trans. Autom. Sci. Eng.* **8** 327–37
[9] Hu L, Zou J, Fu X., Yang Y H, Ruan X D and Wang C Y 2009 A reconstruction approach to determining the magnetic field around an electromagnetic velocity probe *Meas. Sci. Technol.* **20** 015103
[10] Baillet S, Mosher J C and Leahy R M 2001 Electromagnetic brain mapping *IEEE Signal Process. Mag.* **18** 14–30
[11] Hämäläinen M S, Hari R, Ilmoniemi R, Knuutila J and Lounasmaa O 1993 Magnetoencephalography: theory, instrumentation and applications to the noninvasive study of human brain function *Rev. Mod. Phys.* **65** 413–97
[12] Hu C, Meng M Q-H and Mandal M 2005 Efficient magnetic localization and orientation technique for capsule endoscopy *Int. J.Inform. Acquis.* **2** 23–36
[13] Stathopoulos E, Schlageter V, Meyrat B, Ribaupierre Y D and Kucera P 2005 Magnetic pill tracking: a novel non-invasive tool for investigation of human digestive motility *Neurogastroenterol. Motil.* **17** 148–54
[14] Roetenberg D, Slycke P and Veltink P H 2007 Ambulatory position and orientation tracking fusing magnetic and inertial sensing *IEEE Trans. Biomed. Eng.* **54** 883–90
[15] Schepers H M, Roetemberg D and Veltnik P H 2010 Ambulatory human motion tracking by fusion of inertial and magnetic sensing with adaptive actuation *Med. Biol. Eng. Comput.* **48** 27–37
[16] Tsai M-C and Yang C-H 2008 A flux-density-based electromagnetic servo system for real-time magnetic servoing/tracking *IEEE/ASME Trans. Mechatronics* **13** 249–56
[17] Minkov D 2002 Estimating the sizes of surface cracks based on hall element measurements of the leakage magnetic field and a dipole model of a crack *Appl. Phys.* A **74** 169–76
[18] Toliyat H A, Wlas M and Krzemiriski Z 2008 Neural-network-based parameter estimations of induction motors *IEEE Trans. Indust. Electron* **55** 1783–94

[19] Thompson K R, Acarnley P P and French C 2000 Rotor position estimation in a switched reluctance drive using recursive least squares *IEEE Trans. Indust. Electron.* **47** 368–79

[20] Golub G and Pereyra V 2003 Separable nonlinear least squares: the variable projection method and its applications *Inverse Problems* **19** R1–26

[21] Gill P E, Murray W and Saunders M A 2005 SNOPT: an SQP algorithm for large-scale constrained optimization *SIAM Rev.* **12** 99–131

[22] Xu Z L 2000 *Modern Mathematics Handbook: Classical Mathematics* 1st edn (Wuhan, Hubei: Huazhong University of Science and Technology Press)